

---

# DRAFT

## CMS Physics Analysis Summary

*The content of this note is intended for CMS internal use and distribution only*

---

2012/06/13

Head Id: 126036

Archive Id: 129300M

Archive Date: 2012/05/31

Archive Tag: trunk

### Measurement of Spin Correlations in $t\bar{t}$ events in the dilepton channels in pp collisions at $\sqrt{s} = 7$ TeV

The CMS Collaboration

#### Abstract

We present a measurement of the correlation of spins of tops in  $t\bar{t}$  dilepton channels in pp collisions at  $\sqrt{s} = 7$  TeV. The data sample used for the measurement corresponds to an integrated luminosity of  $5.0 \pm 0.1 \text{ fb}^{-1}$  collected with the CMS detector at the LHC. The measurement is performed in events with two leptons (electrons or muons) in the final state, and at least two jets where at least one is identified as a b-jets. In addition the presence of missing transverse energy is required. The spin correlation in  $t\bar{t}$  events are extracted from a fit of the angular distribution between the two selected leptons. The spin correlation in the helicity basis is found to be  $0.23 \pm 0.02 \pm X$ . The spin correlation is also investigated through other variables, for different  $t\bar{t}$  invariant masses, and a good compatibility with the Standard Model is found.

This box is only visible in draft mode. Please make sure the values below make sense.

PDFAuthor: Jeremy Andrea, Thomas Speer, Felix Hoehle, Suharyo Sumowidagdo, Efe Yazgan, Kelly Beernaert, Yanju Tu, Jacob Linacre, Heiko Geenen  
PDFTitle: Measurement of Spin Correlations in  $t\bar{t}$  production  
PDFSubject: CMS  
PDFKeywords: CMS, physics, software, computing

Please also verify that the abstract does not use any user defined symbols



## 1 Introduction

At the LHC, top quarks are produced abundantly, mainly in pairs by gluon fusion. The top quark mass has been measured to be  $172.9 \pm 0.6 \pm 0.9 \text{ GeV}/c^2$  [1] and the width of the top quark is found to be  $\Gamma_t = 2.0_{-0.6}^{+0.7} \text{ GeV}$ [1]. This implies a lifetime much shorter than the hadronization time-scale,  $m_t/\Lambda_{\text{QCD}}^2$ . Therefore, the spin of the top quark at production is transferred to its decay products and can be accessed directly by the distribution of angular observables. This makes a measurement of the spin correlations of the  $t\bar{t}$  pairs possible [2]. The investigation of spin correlations in the  $t\bar{t}$  system probes the bare quark at production, and by this the top pair production processes and perturbative QCD. At the LHC, at low invariant mass of the  $t\bar{t}$  pair, the production is dominated by the fusion of like-helicity gluon pairs, resulting in top pairs in the  $\uparrow\uparrow$  or  $\downarrow\downarrow$  helicity-state. At higher invariant masses, the dominant channel switches to unlike-helicity gluons, producing  $t\bar{t}$  pairs in the  $\uparrow\downarrow$ - or  $\downarrow\uparrow$ -configurations which is identical to the configuration produced by  $q\bar{q}$  annihilation at the Tevatron [3]. In the dileptonic decay through  $t\bar{t} \rightarrow l^+ \nu l^- \bar{\nu} b \bar{b}$ , the charged leptons are correlated in azimuthal angle ( $\Delta\phi(\ell, \ell)$ ) in the laboratory frame [3] and can be measured precisely by the LHC experiments without reconstructing the full event kinematics. CDF and D0 measure the  $t\bar{t}$  spin correlation to be in agreement within SM expectation using template fit methods to angular distributions, as well as performing a template fit [4–6]. The ATLAS experiment reported a measurement of the spin correlation via  $\Delta\phi(\ell, \ell)$  distributions to be in agreement with next-to-leading order SM predictions [7].

This analysis uses an integrated luminosity of  $5 \text{ fb}^{-1}$  of data recorded by the CMS detector[8] from proton-proton collisions at  $\sqrt{s} = 7 \text{ TeV}$  provided by the LHC. The present measurement of the spin correlations in the  $t\bar{t}$  events are compared to the Standard Model (SM) expectation and opposed to the hypothesis, that they are uncorrelated.

In addition to the direct spin correlation measurement via  $\Delta\phi(\ell, \ell)$ , we present the measurement of asymmetries related to the spin correlation.

The description of the data-sets and simulated samples is given in section 2. The baseline event selection is presented in section 3. A short presentation of the data-driven techniques used to estimate the background contamination can be found in section 4, while the description of the systematic effects are discussed in section 5. The measurements are presented in section 6, followed by our conclusion in section 7.

## 2 Simulation of signal and backgrounds

The  $t\bar{t}$  signal events are either simulated with MC@NLO [9] or POWHEG [10] Monte Carlo (MC) packages. Two samples are produced with and without spin-correlations through MC@NLO, while the simulated events through POWHEG contains spin correlation. Parton showering and hadronization of the events is simulated by HERWIG6 [11] for MC@NLO and by PYTHIA [12] for POWHEG. The generated signal with and without spin correlations are processed with the FastSim detector simulation [13], while all other generated events are processed with the GEANT4-based [14] CMS detector simulation. All events are reconstructed using the same software as used for collision data. The samples processed with FastSim detector simulation are validated by comparing distributions obtained from events processed with full detector simulation. The kinematic variables and multiplicities of jets, muons and electrons and derived variables like missing transverse energy and invariant lepton pair masses and the b-tagging CVS discriminator show no differences.

45 For the signal samples, a top quark mass of  $m_{top} = 172.5 \text{ GeV}/c^2$  is assumed. Additional  
 46 samples with and without spin correlations and an assumed top mass of 167.5, 170, 175, and  
 47  $177.5 \text{ GeV}/c^2$  are produced with MC@NLO for systematic uncertainty calculations. Moreover,  
 48 simulations of the  $t\bar{t}$  signal sample with and without spin correlations are also made using  
 49 POWHEG [10] with HERWIG6 and with PYTHIA to estimate systematic uncertainties on  
 50 modeling of signal  $t\bar{t}$  events and of the showering.

51 The main sources of background are  $W/Z$ +jets in which the vector boson decays leptonically,  
 52 and single top quark. The electro-weak production of single top quarks in the  $tW$  channel  
 53 is simulated using POWHEG or PYTHIA. The corresponding cross-section of  $15.7 \pm 0.4 \text{ pb}$  is  
 54 used in this analysis. The  $W/Z$ +jets events are processed using MADGRAPH[15], with up  
 55 to four jets where the jet flavor is inclusive. The corresponding NNLO cross sections, calcu-  
 56 lated by the FEWZ program [16], are  $31.3 \pm 1.6 \text{ nb}$  and  $15.0 \pm 0.77 \text{ nb}$ , respectively. The diboson  
 57 processes,  $WW, WZ, ZZ$ , are generated using PYTHIA or MADGRAPH. The corresponding  
 58 cross sections used in this analysis are  $47.0 \pm 1.7 \text{ pb}$ ,  $18.2 \pm 0.7 \text{ pb}$  and  $7.7 \pm 0.2 \text{ pb}$ , respectively for  
 59 the  $WW, WZ$  and  $ZZ$  events.

60 Among the simulated backgrounds, only the predictions for the diboson and single top quark  
 61 backgrounds are used in the analysis. The normalizations of all other backgrounds are esti-  
 62 mated from data, as discussed in section 4.

63 Finally, the pileup effects are modeled in the simulation by mixing minimum bias events,  
 64 recorded by the CMS detector, to the simulated events with event multiplicities which repro-  
 65 duce the pileup profile of  $pp$  collisions at the LHC.

### 66 3 Event selection

67 The baseline event selection applied for both analyzes, as well as the reconstruction algorithms  
 68 of objects, are presented in this section. Selection requirements which are specific to an analysis  
 69 are discussed in Secs. 6.1 and 6.2.

70 Events in data are collected using dilepton triggers which require the presence of at least two  
 71 muons, two electrons or one electron and one muon in the events, with various threshold on the  
 72 transverse momentum ( $p_T$ ) of the leptons. The efficiency of the trigger selection in data was  
 73 estimated using [17] and the trigger efficiency in the simulation is corrected with the corre-  
 74 sponding data-to-MC scale factors of  $0.977 \pm 0.015$ ,  $0.962 \pm 0.016$  and  $1.008 \pm 0.009$  for the  $\mu^+\mu^-$ ,  
 75  $e^+e^-$  and  $e^\pm\mu^\mp$  channels respectively.

76 After requiring the presence of a good primary vertex in the events, with a distance to the  
 77 center of the detector  $< 24 \text{ cm}$  along the axis of the beam line and within  $2 \text{ cm}$  in the transverse  
 78 plan, at least two reconstructed leptons with opposite electric charge in the event are required.  
 79 The electrons are reconstructed by associating tracks from the inner tracker with calorimetric  
 80 clusters in the electromagnetic calorimeter. Muons are reconstructed by matching tracks from  
 81 the outer muon detector to the tracks reconstructed by the inner tracker. To reject jets or hadrons  
 82 wrongly reconstructed as leptons, specific lepton identification criteria are applied on both  
 83 lepton flavor [18, 19].

84 The leptons are required to have  $p_T > 20 \text{ GeV}$  and to satisfy  $|\eta| < 2.1$  and  $|\eta| < 2.5$  for elec-  
 85 trons and muons respectively. The track of the lepton candidates are required to have an origin  
 86 compatible with the primary vertex position, and further quality requirements are applied [17].  
 87 Leptons coming from  $W$  decays (excluding the  $\tau$ ) are expected to be isolated from any other  
 88 particles. Thus, lepton candidates are required to be isolated from other activities in the tracker,

89 or in the calorimeter. A cone of  $\Delta R = 0.3$  (with  $\Delta R = \sqrt{\Delta\phi^2 + \Delta\eta^2}$ ), constructed around the  
 90 lepton directions, is used to collect the transverse energy deposited close to the lepton, ex-  
 91 cluding the contribution for the lepton candidate. The energy deposition in the cone is esti-  
 92 mated using Particle-Flow (PF) candidates [20], excluding PF candidates associated to pileup  
 93 events. The ratio of the sum of the transverse energy deposited within the cone to the  $p_T$  of the  
 94 lepton candidate defines the lepton isolation  $I_{rel}$ . The lepton candidates are rejected if they do  
 95 not satisfy  $I_{rel} < 0.17$  and  $I_{rel} < 0.20$  for electrons and muons respectively.

96 Lepton reconstruction efficiencies are close to 100% [18, 19]. The lepton selection efficiencies are  
 97 estimated with a tag&probe method elsewhere [17, 21] as a function of  $p_T$  and  $\eta$  of the leptons.  
 98 Comparing the lepton selection efficiencies in data and the simulation, inclusive data-to-MC  
 99 scale factors of  $0.997 \pm 0.005$ ,  $0.995 \pm 0.005$  and  $0.994 \pm 0.005$  are found for  $t\bar{t}$  signal events. In  
 100 order to reject Drell-Yan events, the dilepton invariant mass is required to be outside the range  
 101 [76, 106] GeV.

102 The jets are reconstructed from PF candidates [20] using an anti- $k_T$  algorithm [22] with a cone  
 103 size of 0.5. The charged particles coming from pileup events are rejected by requiring the PF  
 104 candidates to be associated to the main primary vertex. The neutral component from pileup  
 105 events are accounted using the so called area-based procedure described in [23, 24].

106 B jets from top decays are identified as originating from the hadronization of a b-quark using  
 107 the "Combined Secondary Vertex" algorithm [25]. The performance of the b-tagging selection  
 108 are estimated using QCD-multi-jets events as described in [26].

109 Because of the presence of escaping neutrinos in  $t\bar{t}$  signal events, the transverse missing energy  
 110  $E_{\cancel{T}}$  can either be used to reject backgrounds like  $Z/\gamma^*$  events or for the reconstruction of  $t\bar{t}$   
 111 events. The  $E_{\cancel{T}}$  vector is defined as  $E_{\cancel{T}} = -\sum_i p_T^i$ , where the sum is done over the PF candidates,  
 112 excluding those coming from pileup events [27]. The  $E_{\cancel{T}}$  is then the norm of  $E_{\cancel{T}}$  vector.

113 The thresholds applied on the b-tagging discriminator and on the  $E_{\cancel{T}}$  are discussed in Secs.6.1  
 114 and 6.2.

## 115 4 Background estimates

116 Two different kinds of backgrounds are considered. The first kind is production of DY lepton  
 117 pair events,  $e^+e^-$  and  $\mu^+\mu^-$ . The second kind of production of W-like and QCD multi-jets  
 118 events that have one or two non-prompt leptons, not coming from W or Z  $Z/\gamma^*$  decays. A  
 119 more detailed description can be found in [17, 28, 29].

120 The DY background is dominant in the  $e^+e^-$  and  $\mu^+\mu^-$  channels. It is estimated from the number  
 121 of events in data inside the dilepton invariant mass window of  $76 \text{ GeV}/c^2 < m_{\ell\ell} < 106 \text{ GeV}/c^2$ ,  
 122 scaled by the ratio of events that fail and pass this selection.

123 The non-prompt lepton backgrounds are estimated by first defining a looser definition of lepton  
 124 isolation. Then different dilepton samples are constructed. The first (loose) sample contain  
 125 events that has two loose leptons, the second (medium) sample contain events that has at least  
 126 one tight lepton, and the third (tight) sample contain events that has two tight leptons.

127 By introducing the probability for prompt lepton and non-prompt lepton to pass the loose and  
 128 tight isolation criteria, one can construct a system of linear equations with the number of events  
 129 with two prompt-lepton ( $t\bar{t}$  and DY) and events with one or two prompt leptons as unknown.  
 130 Solving this system of linear equations yield the expected background from W-like events and  
 131 QCD multi-jet [17]. This method is known as matrix method in the literature [30] or Barlow's

132 event reweighting method [31]. Another similar method [28], based on the rate of non-prompt  
 133 leptons, is used in Sec.6.2.

## 134 5 Systematic uncertainties

135 Various systematic effects are affecting the measurements. Some of them are related to detector  
 136 effect, others are related to the modeling of  $t\bar{t}$  signal events. The main sources of systematic  
 137 uncertainties are listed below.

138 The experimental systematic effects are :

- 139 • **Uncertainty on the lepton selection** : uncertainties on the dilepton trigger and lep-  
 140 ton selection (isolation and identification) affect the normalization of signal and  
 141 background events, but also have some influence on the shapes of of angular dis-  
 142 tributions of leptons. The corresponding effects on the measurements are estimated  
 143 by changing the scale-factors within their uncertainties.
- 144 • **Lepton energy scale** : the uncertainty on lepton energy scale, which affects mainly  
 145 the  $p_T$  distribution of leptons, is of 0.3% for electrons and negligible for muons, as  
 146 estimated from comparisons between data and simulated Z events. The correspond-  
 147 ing systematic uncertainty on the measurements are estimated by performing the fit  
 148 with the energy scale of electrons varied by  $\pm 0.3\%$ .
- 149 • **Jet energy scale and jet energy resolution** : the uncertainty from the jet energy  
 150 scale (JES) correction is first estimated by variation the JES of jets within their un-  
 151 certainties, with the proper propagation to the  $E_T$ . The jet energy resolution (JER) is  
 152 estimated similarly, but by varying the JER by 5 to 10%, depending on the  $\eta$  of the  
 153 jet.
- 154 • **Background events** : the uncertainty on the normalization of backgrounds is con-  
 155 sidered by varying the background contamination by 50 or 100%, depending on the  
 156 selection applied.
- 157 • **Uncertainty on the pileup modeling** : the uncertainty of 8% on the proton-proton  
 158 cross section at the LHC energy of 7 TeV influence the pileup modeling and is used  
 159 to estimate the corresponding systematics.

160 The systematic uncertainties related to the modeling of  $t\bar{t}$  signal events :

- 161 • **Systematic related to the generator** : the uncertainty related to the use of a given  
 162 generator is estimated by using different  $t\bar{t}$  samples produced with POWHEGor  
 163 MCNLO. In both samples, HERWIG is used for the hadronization and the frag-  
 164 mentation.
- 165 • **Systematic related to hadronization and fragmentation** : the uncertainty on the  
 166 fragmentation and hadronization modeling is estimated by using two different  $t\bar{t}$   
 167 samples produced with POWHEG but with different the hadronization and frag-  
 168 mentation performed by either HERWIGor PYTHIA.
- 169 • **Systematic related to the top quark mass**: the uncertainty on the top quark mass  
 170 is estimated using  $t\bar{t}$  signal events with generated with different top masses, as dis-  
 171 cussed in Sec.2, assuming a uncertainty on the top mass of 2 GeV around  $m_t = 172.5$   
 172 GeV.
- 173 • **PDF** : the uncertainty related to PDF are estimated by using the procedure defined  
 174 in Ref.[32].

## 6 Measurement of spin correlations in $t\bar{t}$ events

### 6.1 Spin correlation using $\Delta\Phi$ distributions

The angular difference in the azimuthal plane between the two leptons coming from the  $W$  decays in  $t\bar{t}$  events ( $\Delta\phi = |\phi_{l1} - \phi_{l2}|$ ) is sensitive to the spin correlation of the two top quarks. The spin correlation is estimated by fitting the  $\Delta\phi$  distribution observed in data.

The fit is performed using a data-set constituted of events passing the baseline selection described in Sec.3. The events are also required to have a dilepton invariant mass above 20 GeV for the three channels and a  $E_T$  above 40 GeV for the  $e^+e^-$  and  $\mu^+\mu^-$  channels only. In addition, at least one of the selected jet should pass the loose working point of the Combined Secondary Vertex  $b$  tagging algorithm. The loose working point corresponds to a  $b$ -tagging efficiency of 80-85% for a mis-tagging rate of about 10%, as estimated from the simulation.

A comparison of the  $\Delta\phi$  distributions in  $t\bar{t}$  events simulated with MCNLO with and without spin correlation can be seen on Fig.1.

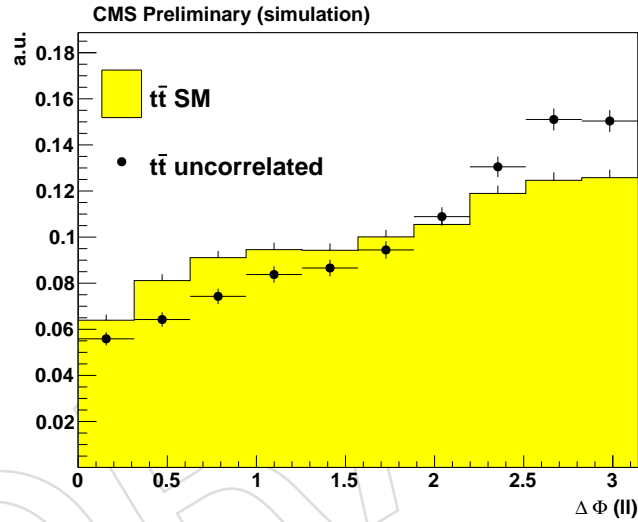


Figure 1:  $\Delta\phi$  (ll) distributions for  $t\bar{t}$  signal events with spin correlation compatible with the SM, and without correlation (uncorrelated). The three channels are summed after the event selection.

The spin correlation is defined as the difference between the number of  $t\bar{t}$  events with spin orientation of top quarks aligned and anti-aligned, divided by the total number of  $t\bar{t}$  events, namely :

$$A = \frac{N(\uparrow\uparrow) + N(\downarrow\downarrow) - N(\downarrow\uparrow) - N(\uparrow\downarrow)}{N(\uparrow\uparrow) + N(\downarrow\downarrow) + N(\downarrow\uparrow) + N(\uparrow\downarrow)}, \quad (1)$$

where the arrows are referring to the orientation of the spin of the top and anti-top quarks with respect to the chosen quantization axis.

The analysis follows the same strategy than the one described in Ref.[7]. The spin correlation is estimated from the  $\Delta\phi$  distribution observed in data, by means of a template fit. Three different templates are considered: the  $\Delta\phi$  distributions from simulated  $t\bar{t}$  events with and without spin

196 correlations between the top quarks, and a  $\Delta\phi$  distribution which describe the background  
 197 events.

198 A binned likelihood fit method is used, as implemented in RooFit, to perform a simultaneous  
 199 fit of the  $ee$ ,  $\mu\mu$  and  $e\mu$  channels. All the events are fitted together in a single likelihood fit, but  
 200 different templates are used according to the decay channel ( $e^+e^-$ ,  $\mu^+\mu^-$  and  $e^\pm\mu^\mp$ ). A single  
 201 template per decay channel is used to describe the background events, where the templates  
 202 for each background process are summed. The templates are derived from the simulation, and  
 203 weighted by the data-driven estimates for the  $Z/\gamma^*$  and non-prompt lepton background, and  
 204 the prediction from the simulation for the single top quark and the diboson backgrounds.

205 The templates for  $t\bar{t}$  signal events are derived from the MCNLO events produced with and  
 206 without spin correlation. The number of  $t\bar{t}$  signal events in each decay channel are parameters  
 207 of the fit, as well as the fraction  $f$  of events with spin correlation. The parameter  $f$  is the same  
 208 for the three channels. With the top spin correlation used in the MCNLO simulation,  $A_{SM}$ , the  
 209 measured spin correlation is  $f \times A_{SM}$ .

210 The bias of this method is determined using ensembles of pseudo-experiments based on the  
 211 expected numbers of signal and background events, for different hypothesis of spin correlation  
 212  $f$  from -1 to 2. No bias is observed on the measured fraction. The width of the pull distribution  
 213 is within 10% of unity over the whole range, and the average pull width is used to rescale the  
 214 statistical uncertainty.

215 The result of the fit performed on data is shown in Fig 2. The number of  $t\bar{t}$  signal is measured  
 216 to be  $1726.2 \pm 44.3$  in the  $e^+e^-$  channel,  $2153.3 \pm 50.0$  in the  $\mu^+\mu^-$  channel and  $6404.7 \pm 84.5$   
 217 in the  $e^\pm\mu^\mp$  channel. The fraction of spin correlation  $f$  is measured to be  $0.74 \pm 0.07$ . The  
 218 uncertainties are statistical only. The total number of background events, dominated by the  
 219  $Z/\gamma^*$  processes, are  $241.4 \pm 120.7$ ,  $349.2 \pm 174.8$  and  $742.7 \pm 371.4$  for the  $e^+e^-$ ,  $\mu^+\mu^-$  and  
 220  $e^\pm\mu^\mp$  channels respectively. The results of the fit, for the combination of the three channels, can  
 221 be seen on Fig.2.

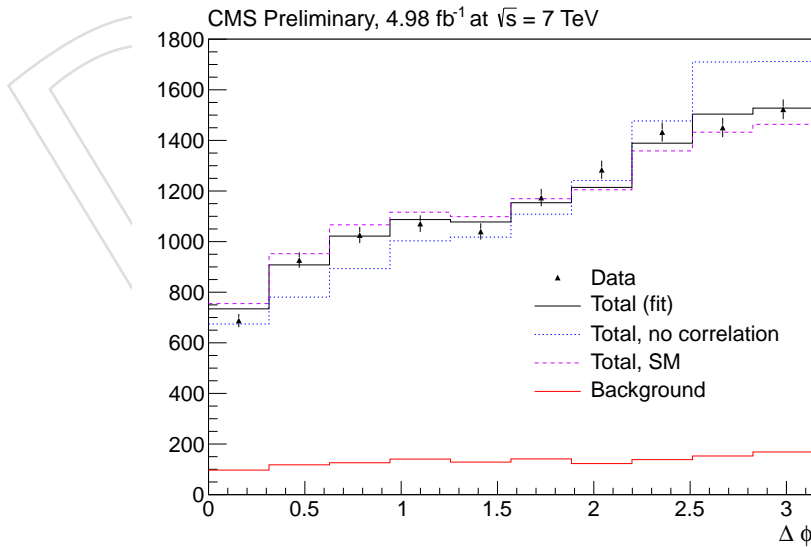


Figure 2: Result of the fit (solid line) performed on data (triangles) after the combination of the three channels. The data are also compared to the  $\Delta\phi$  distribution of  $t\bar{t}$  events with and without spin correlation. The background components are included in the plot.

222 The systematic uncertainties are estimated using pseudo-experiments, where the shapes of dis-  
 223 tributions used to create pseudo-data are fluctuated according to the systematic effect under  
 224 study.

225 For each source, pseudo-experiments are generated from MC event samples for which the rel-  
 226 evant parameters are varied, and fit with the templates derived with the nominal parameters.  
 227 The average variation of the spin correlation is used to estimate the systematic uncertainty.

228 In the helicity basis, the spin correlation, as defined in Eq.1, is expected to be  $A_{hel}^{SM} = 0.31$  in the  
 229 Standard Model [7]. The measurement yields a spin correlation of  $A_{hel}^{meas} = 0.23 \pm 0.02 \pm X$  in  
 230 the helicity basis.

## 231 6.2 Measurement of asymmetries related to the spin correlation

### 232 6.2.1 Inclusive measurement

233 In this note, in addition to the spin correlation measurement, we also present the measurement  
 234 of the following asymmetries related to the spin correlation, inspired by a recent paper by  
 235 Krohn, Liu, Shelton, and Wang [33]:

- 

$$A_{\Delta\phi} = \frac{N(\phi_{l+l-} < \pi/2) - N(\Delta\phi_{l+l-} > \pi/2)}{N(\phi_{l+l-} < \pi/2) + N(\Delta\phi_{l+l-} > \pi/2)}$$

236 where  $\Delta\phi$  is the azimuthal angle between the two leptons, as defined in the previous  
 237 section.

- 

$$A_{c1c2} = \frac{N(\cos(\theta_l^+) \times \cos(\theta_l^-) > 0) - N(\cos(\theta_l^+) \times \cos(\theta_l^-) < 0)}{N(\cos(\theta_l^+) \times \cos(\theta_l^-) > 0) + N(\cos(\theta_l^+) \times \cos(\theta_l^-) < 0)}$$

238 where  $\theta_l$  is the production angle of the lepton with respect to the direction of the  
 239 parent top or anti-top in the  $t\bar{t}$  rest frame. This quantity gives a direct measure of the  
 240 spin correlation.

241 In order to further reduce the background which dilutes the asymmetries, while keeping the  
 242 efficiency of selecting  $t\bar{t}$  events, in addition to the baseline event selection described in Section 3,  
 243 addition requirements are added. First, at least one of the jets are required to be consistent with  
 244 coming from the decay of heavy flavor hadrons and be identified as b jets by the CSVM b-  
 245 tagging algorithm [25]. The  $E_T$  in the event is required to exceed 30 GeV in all three channels,  
 246 consistent with the presence of two undetected neutrinos. The events with dilepton invariant  
 247 mass  $< 12 \text{ GeV}/c^2$  are removed to remove events with Upsilon. The muon  $|\eta|$  is up to 2.4.

248 With this event selections, the MC predicts that the sample is dominated by  $t\bar{t} \rightarrow \ell^+\ell^-$  (92%),  
 249 with the largest background coming from single top production. The data driven methods de-  
 250 scribed in Section 4 are used to cross-check the MC estimates for the background contributions  
 251 from events with fake leptons,  $Z/\gamma^* \rightarrow e^+e^-$  and  $Z/\gamma^* \rightarrow \mu^+\mu^-$  events. The data-driven  
 252 prediction is consistent with the MC estimates within the uncertainties. Therefore, in the fol-  
 253 lowing, we rely on MC for the background estimate and assign the systematics from the data-  
 254 driven background estimate. The MC samples are described in section 2, where the  $t\bar{t} \rightarrow \ell^+\ell^-$   
 255 component is taken from the POWHEG-PYTHIA  $t\bar{t}$  sample. The MC yields are normalized to 4.98  
 256  $\text{fb}^{-1}$  using the cross sections from Section 2. The  $t\bar{t} \rightarrow \ell^+\ell^-$  yields are normalized to make the  
 257 total MC match the data.

258 The observable  $A_{\Delta\phi}$  is purely leptonic, but the observable  $A_{c1c2}$  requires the reconstruction of  
 259 the  $t\bar{t}$  system. Each event has two neutrinos resulting in a ambiguity. Moreover, there is a

260 combinatorial ambiguity in the assignment of the b-jets to the decay branches. The analytical  
 261 matrix weighting technique [34] is used to find a probable solution. Each event is reconstructed  
 262 using a range of possible  $m_t$  values from 100-300 GeV/ $c^2$  in 1 GeV/ $c^2$  steps. The  $m_t$  hypothesis  
 263 with the maximum averaged weight over possible solutions is taken, and the  $t\bar{t}$  kinematics  
 264 are then taken from the solution with largest weight. Approximately 17% of events have no  
 265 solution, and are not used in the measurements of  $A_{c1c2}$ .

266 New physics is expected to be more prominent at high  $t\bar{t}$  invariant mass,  $M_{t\bar{t}}$ . We thus compare  
 267 the data to the simulation for  $A_{\Delta\phi}$  and  $A_{c1c2}$  both before and after requiring  $M_{t\bar{t}} > 450$  GeV/ $c^2$ .  
 268 The results are shown in Figures 3 and 4, and the corresponding reconstruction-level asymmetries  
 269 are summarized in Table 2. Agreement between the data and the simulation is observed  
 270 in both the inclusive and high- $M_{t\bar{t}}$  regions.

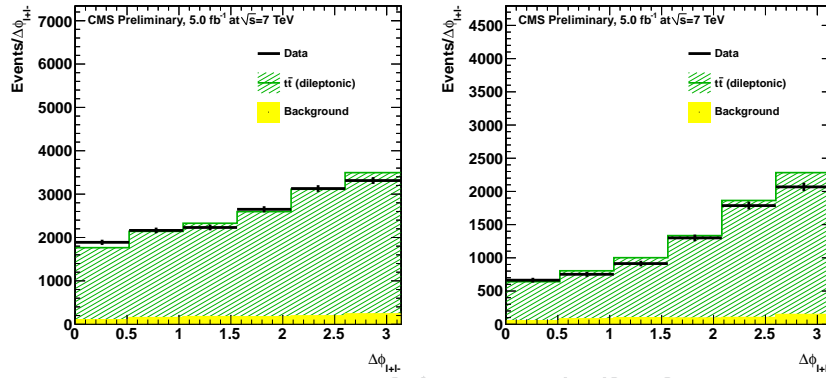


Figure 3: Reconstruction level asymmetry distributions for  $A_{\Delta\phi}$ , inclusively (left) and in the region where  $M_{t\bar{t}} > 450$  GeV/ $c^2$  (right). The  $t\bar{t} \rightarrow l^+l^-$  component is taken from the POWHEG-PYTHIA  $t\bar{t}$  sample. The  $t\bar{t} \rightarrow l^+l^-$  yields are normalized to match the data in the inclusive measurement.

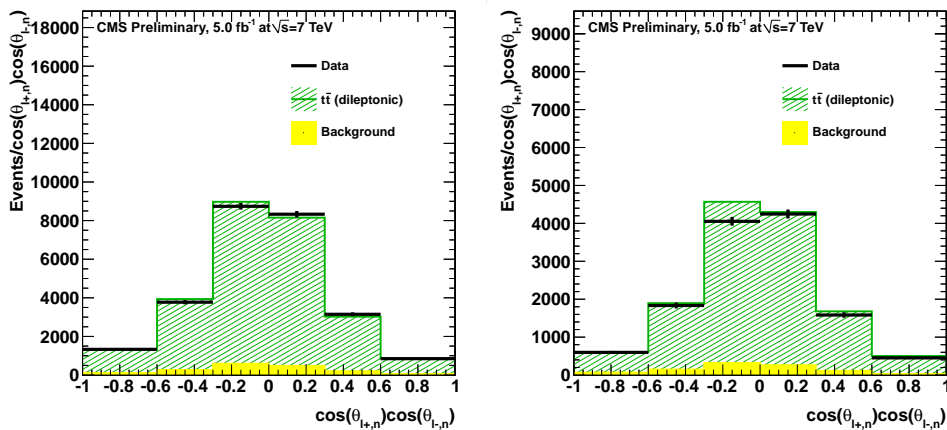


Figure 4: Reconstruction level asymmetry distributions for  $A_{c1c2}$ , inclusively (left) and in the region where  $M_{t\bar{t}} > 450$  GeV/ $c^2$  (right). The  $t\bar{t} \rightarrow l^+l^-$  component is taken from the POWHEG-PYTHIA  $t\bar{t}$  sample. The  $t\bar{t} \rightarrow l^+l^-$  yields are normalized to match the data in the inclusive measurement.

systematic	absolute	relative (%)
statistic uncertainty	0.07	9%
MC stat uncertainty	0.06	8%
	experimental	
Lepton SF	0.02	3%
Lepton energy scale	0.01	2%
JES/JER	0.05	7%
all backgrounds	0.04	5%
PU	0.03	4%
b-tagging	-	-
	t $\bar{t}$ modeling	-
MC statistic	-	-
generator	-	-
hadr. and frag.	-	-
top mass	-	-
PDF	-	-

Table 1:

Table 2: Reconstructed and simulated asymmetries, inclusively and in the region where  $M_{t\bar{t}} > 450 \text{ GeV}/c^2$ . Uncertainties are statistical only.

Reconstructed asymmetries	Data	Simulation
$A_{\Delta\phi}$ , inclusive region	$-0.158 \pm 0.010$	$-0.171 \pm 0.002$
$A_{c1c2}$ , inclusive region	$-0.062 \pm 0.011$	$-0.087 \pm 0.002$
$A_{\Delta\phi}$ , $M_{t\bar{t}} > 450 \text{ GeV}/c^2$	$-0.378 \pm 0.019$	$-0.384 \pm 0.003$
$A_{c1c2}$ , $M_{t\bar{t}} > 450 \text{ GeV}/c^2$	$-0.019 \pm 0.016$	$-0.044 \pm 0.003$

## 271 6.2.2 Unfolding

272 The reconstructed asymmetries are distorted from the true underlying distributions by the limited  
 273 acceptance of our detector and by bin-to-bin smearing due to a finite resolution of these  
 274 variables. We have developed a procedure that allows us to correct the binned data for both effects,  
 275 yielding “parton-level” distributions and asymmetries. These distributions represent the  
 276 differential cross-sections in the variables of interest, and are normalized to unity. The details  
 277 of the procedure are described in [35].

278 The inclusive data sample is used for the unfolded results (i.e. no  $M_{t\bar{t}}$  cut), although any bias  
 279 from acceptance effects is removed by the unfolding procedure. The  $t\bar{t}$  parton-level prediction  
 280 is obtained from POWHEG-PYTHIA simulated events. The background-subtracted and unfolded  
 281 differential cross-sections for  $\Delta\phi_{l+l-}$  and  $\cos(\theta_l^+) \times \cos(\theta_l^-)$  are shown in Figure 5. The  
 282 asymmetries measured from these unfolded distributions are also parton-level quantities. The  
 283 unfolded value of  $A_{\Delta\phi}$  is  $-0.097 \pm 0.015 \pm 0.026$  in data and  $-0.119 \pm 0.0004$  in the simulation.  
 284 The unfolded value of  $A_{c_1c_2}$  is  $-0.015 \pm 0.037 \pm 0.046$  in data and  $-0.063 \pm 0.0004$  in the  
 285 simulation. The systematic uncertainties are from the sources described in Table 3.

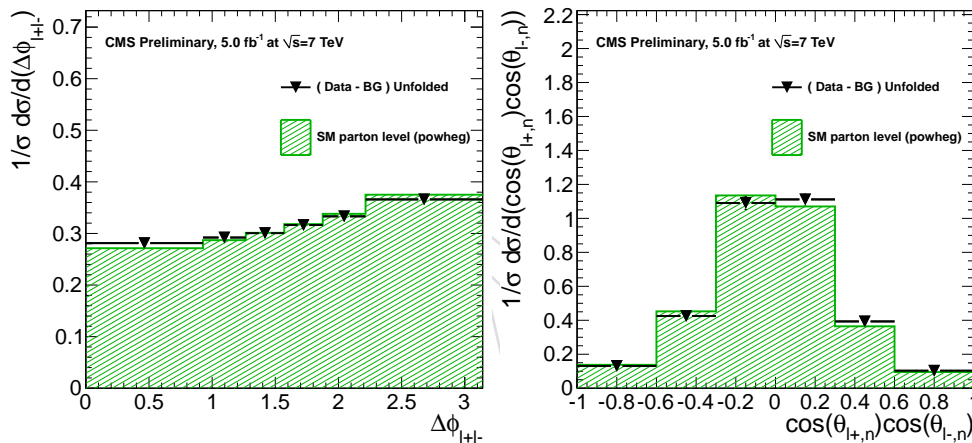


Figure 5: Background-subtracted and unfolded asymmetry distributions.

## 286 7 Conclusion

287 This note presents investigations of top spin correlation in  $t\bar{t}$  dilepton final state ( $e^+e^-$ ,  $\mu^+\mu^-$  and  
 288  $e^\pm\mu^\mp$ ). The spin correlation in the helicity basis is found to be  $A_{hel.}^{meas.} = 0.23 \pm 0.02 \pm X$ . The  
 289 spin correlation is also investigated in various  $m_{t\bar{t}}$  ranges through the forward-background  
 290 asymmetries. The results are in agreement with the SM predictions.

## 291 References

- 292 [1] Particle Data Group Collaboration, “Review of particle physics: ”, *J. Phys.* **G37** (2010 and  
 293 2011 partial update for the 2012 edition) 075021,  
 294 doi:10.1088/0954-3899/37/7A/075021.
- 295 [2] M. Beneke et al., “Top Quark Physics”, arXiv:0003033.
- 296 [3] G. Mahlon and S. Parke, “Spin Correlation Effects in Top Quark Pair Production at the  
 297 LHC”, *Phys. Rev.* **D81** (2010) 074024, doi:10.1103/PhysRevD.81.074024.

systematic	$A_{\Delta\phi}$	$A_{c1c2}$
statistic uncertainty	0.015	0.037
MC stat uncertainty	0.0004	0.0004
	experimental	
Lepton SF	0.0	0.0
Lepton energy scale	-	-
JES/JER	0.009	0.043
all backgrounds	0.002	0.009
PU	0.003	0.002
Unfolding	0.002	0.009
$b$ -tagging	0.001	0.001
	$t\bar{t}$ modeling	
MC statistic	-	-
generator	0.024	0.014
hadr. and frag.	-	-
top mass	0.002	0.019
PDF	-	-

Table 3:

- 298 [4] CDF Collaboration, “Measurement of  $t\bar{t}$  Spin Correlation in  $p\bar{p}$  Collisions Using the CDF  
299 II Detector at the Tevatron”, *Phys. Rev.* **D83** (2011) 031104,  
300 doi:10.1103/PhysRevD.83.031104.
- 301 [5] D0 Collaboration, “Measurement of Spin Correlation in  $t\bar{t}$  Production Using a Matrix  
302 Element Approach”, *Phys. Rev. Lett.* **107** (2011) 032001,  
303 doi:10.1103/PhysRevLett.107.032001.
- 304 [6] D0 Collaboration, “Measurement of Spin Correlation in  $t\bar{t}$  Production Using Dilepton  
305 Final States.”, *Phys. Lett.* **B702** (2011) 16, doi:10.1016/j.physletb.2011.05.077.
- 306 [7] Atlas Collaboration, “Observation of spin correlation in  $t\bar{t}$  events from  $pp$  collisions at  
307  $\sqrt{s} = 7$  TeV using the ATLAS detector”, arXiv:arXiv:1203.4081v1.
- 308 [8] CMS Collaboration, “CMS technical design report, volume II: Physics performance”, *J.*  
309 *Phys. G* **34** (2007) 995–1579, doi:10.1088/0954-3899/34/6/S01.
- 310 [9] S. Frixione and B. R. Webber, “Matching NLO QCD computations and parton shower  
311 simulations”, *Journal of High Energy Physics* **2002** (2002), no. 06, 029.
- 312 [10] S. Frixione, P. Nason, and C. Oleari, “Matching NLO QCD computations with parton  
313 shower simulations: the POWHEG method”, *JHEP* **11** (2007) 070,  
314 doi:10.1088/1126-6708/2007/11/070, arXiv:0709.2092.
- 315 [11] G. Corcella et al., “HERWIG 6.5 release note”, arXiv:hep-ph/0210213.
- 316 [12] T. Sjöstrand, S. Mrenna, and P. Skands, “PYTHIA 6.4 physics and manual”, *JHEP* **05**  
317 (2006) 026, arXiv:hep-ph/0603175.
- 318 [13] CMS Collaboration, “Comparison of the Fast Simulation of CMS with the first LHC  
319 data”, (2011).

- 320 [14] J. Allison et al., "Geant4 developments and applications", *IEEE Trans. Nucl. Sci.* **53** (2006)  
321 270, doi:10.1109/TNS.2006.869826.
- 322 [15] F. Maltoni and T. Stelzer, "MadEvent: Automatic event generation with MadGraph",  
323 *JHEP* **02** (2003) 027, arXiv:hep-ph/0208156.
- 324 [16] K. Melnikov and F. Petriello, "Electroweak gauge boson production at hadron colliders  
325 through  $O(\alpha_s^2)$ ", *Phys. Rev.* **D74** (2006) 114017, doi:10.1103/PhysRevD.74.114017,  
326 arXiv:hep-ph/0609070.
- 327 [17] "Measurement of the  $t\bar{t}$  production cross section in the dilepton channel in pp collisions  
328 at  $\sqrt{s} = 7$  TeV", *CMS Physics Analysis Summary* **CMS PAS TOP-11-005** (2011).
- 329 [18] CMS Collaboration, "Electron reconstruction and identification at  $\sqrt{s}=7$  TeV", *CMS*  
330 *Physics Analysis Summary* **CMS-PAS-EGM-10-004** (2010).
- 331 [19] CMS Collaboration, "Performance of the muon identification in pp collisions at  $\sqrt{s}=7$   
332 TeV", *CMS Physics Analysis Summary* **CMS-PAS-EGM-10-004** (2010).
- 333 [20] CMS Collaboration, "Commissioning of the Particle-Flow reconstruction in  
334 Minimum-Bias and Jet Events from pp Collisions at 7 TeV", *CMS Physics Analysis*  
335 *Summary* **CMS-PAS-PFT-10-002** (2010).
- 336 [21] CMS Collaboration, "Measurement of the inclusive W and Z production cross sections in  
337 pp collisions at  $\sqrt{s} = 7$  TeV with the CMS experiment", *J. High Energy Phys* **10** (2011)  
338 007, arXiv:1108.0566.
- 339 [22] M. Cacciari, G. P. Salam, and G. Soyez, "The anti- $k_t$  jet clustering algorithm", *JHEP* **04**  
340 (2008) 063, doi:10.1088/1126-6708/2008/04/063, arXiv:0802.1189.
- 341 [23] M. Cacciari, G. Salam, and G. Soyez, "The Catchment Area of Jets", *JHEP* **04** (2008) 005,  
342 doi:10.1088/1126-6708/2008/04/05, arXiv:0802.1188.
- 343 [24] M. Cacciari and G. Salam, "Pileup subtraction using jet areas", *Phys. Lett.* **B659** (2008)  
344 119, doi:10.1016/j.physletb.2007.09.077, arXiv:0707.1378.
- 345 [25] CMS Collaboration, "b-Jet Identification in the CMS Experiment", *CMS Physics Analysis*  
346 *Summary* **CMS-PAS-BTV-11-004** (2012).
- 347 [26] CMS Collaboration, "Performance of the b-jet identification in CMS", *CMS Physics*  
348 *Analysis Summary* **CMS-PAS-BTV-11-001** (2011).
- 349 [27] CMS Collaboration, "CMS MET Performance in Events Containing Electroweak Bosons  
350 from pp Collisions at  $\sqrt{s} = 7$  TeV", *CMS Physics Analysis Summary*  
351 **CMS-PAS-JME-10-005** (2010).
- 352 [28] CMS Collaboration, "First Measurement of the cross section for Top-Quark Pair  
353 Production in Proton-Proton Collisions at  $\sqrt{s}=7$  TeV", *Phys. Lett.* **B695** (2011) 424,  
354 doi:10.1016/j.physletb.2010.11.058, arXiv:1010.5994.
- 355 [29] CMS Collaboration, "Measurement of the  $t\bar{t}$  production cross section and the top quark  
356 mass in the dilepton channel in pp collisions at  $\sqrt{s} = 7$  TeV", *JHEP* **1107** (2011) 049,  
357 arXiv:1105.5661.

- 358 [30] D0 Collaboration Collaboration, “Measurement of the  $t\bar{t}$  production cross section in  $p\bar{p}$   
359 collisions at  $\sqrt{s} = 1.96$ -TeV using secondary vertex b tagging”, *Phys.Rev.* **D74** (2006)  
360 112004, arXiv:hep-ex/0611002.
- 361 [31] R. J. Barlow, “Event classification using weighting methods”, *J.Comput.Phys.* **72** (1987)  
362 202–219, doi:10.1016/0021-9991(87)90078-7.
- 363 [32] . <http://www.hep.ucl.ac.uk/pdf4lh/>.
- 364 [33] D. Krohn, T. Liu, J. Shelton et al., “A Polarized View of the Top Asymmetry”, *Phys.Rev.*  
365 **D84** (2011) 074034, doi:10.1103/PhysRevD.84.074034, arXiv:1105.3743.
- 366 [34] CMS Collaboration Collaboration, “Measurement of the  $t\bar{t}$  production cross section  
367 and the top quark mass in the dilepton channel in pp collisions at  $\sqrt{s} = 7$  TeV”, *JHEP*  
368 **1107** (2011) 049, arXiv:1105.5661.
- 369 [35] CMS Collaboration, “Measurement of the top polarization in the dilepton channel”,  
370 *CMS Physics Analysis Summary CMS-PAS-TOP-12-016* (2012).

DRAFT